Spatial and Temporal Data Management for the Probabilistic Landslide Hazard Assessment Considering Landslide Typology

J.L.Zêzere, M.L.Rodrigues, E.Reis, R.Garcia, S.Oliveira, G.Vieira & A.B.Ferreira
Centro de Estudos Geográficos, Universidade de Lisboa, Portugal

ABSTRACT: A general methodology for the probabilistic assessment of rotational slide hazard at a regional scale is applied in a test site in the north of Lisbon (Portugal). Landslide susceptibility is assessed using algorithms based on statistical/probabilistic analysis applied over unique-condition terrain units, in a GIS environment. Results of susceptibility predictions are validated by partitioning the landslide data-set using temporal, spatial and random criteria. Prediction-rate curves are used for the quantitative interpretation and classification of the susceptibility map. Integration of triggering information in the modeling procedure is based on the assumption that the same rainfall patterns (quantity/duration), which produced slope instability in the past, will produce the same effects in the future. The landslide hazard is the probability of each pixel to be affected by a slope movement, and results from the coupling between the susceptibility map, prediction-rate curve and return periods of critical rainfall events, on a scenario basis.

1 INTRODUCTION

Most landslide 'hazard' assessments developed worldwide at a regional scale are based on the assumption that future slope movements are more likely to occur under conditions similar to those that led to past landslides (Hansen, 1984; Hutchinson, 1995; Soeters & Van Westen, 1996; Carrara et al., 1998; Aleotti & Choudhury, 1999). However, most 'hazard' maps only provide the classification of susceptibility (or 'spatial probability') not including the temporal component of the hazard, as defined by Varnes et al. (1984). Furthermore, the predictive power of the susceptibility assessment with respect to future landslides needs to be evaluated in order to achieve comprehensive results, which can be easily integrated with vulnerability data within the landslide risk assessment procedure (Chung & Fabbri, 2003; Zêzere et al., 2004).

In the present study a general methodology for the probabilistic assessment of landslide hazard at a regional scale is applied in a test site (18 km^2) located in the north of Lisbon (Portugal).

2 THE STUDY AREA

The Fanhões-Trancão test site is located 20 km northward from the city of Lisbon. The area includes six main geological units, dated from the Upper Barremian-Aptian to the Paleogene (Fig. 1). Most of the geological formations are heterogeneous from the lithological point of view, namely the Albian-Middle Cenomanian rocks (marls, with clay, marly limestone and limestone intercalations) and the Upper Cretaceous Volcanic Complex (compact basalts, weathered basalts and other basic volcanic rocks, and volcanic tuffs). In the south part of the test site Quaternary terrace deposits can be found, partially filling the Loures basin.

The geological structure is a monocline dipping towards the south and southeast (mean dip of strata = 12°). The geological setting strongly controls the regional geomorphology, which is marked by the presence of *cuestas*. The study area is located in the dip slope of the Lousa-Bucelas *cuesta* and includes two main cataclinal valleys: the valley of the Fanhões River in the west, and the deep valley of the Trancão River in the east (Fig. 1).

The detailed geomorphological survey of the study area showed 147 slope movements, which were mapped and included in a database. The verification that different landslide types have different correlations with both landslide conditioning and triggering factors (Zêzere et al., 1999) justifies partitioning the landslide database in three sub-sets based on landslide typology: rotational slides, deep translational slides, and shallow translational slides. This study focus only on the rotational movements, a landslide group that represents 14% of the total landslides, but corresponds to 31% of the total unstable area. Most of these landslides (76%) occurred during the last 25

years. Although the relatively small sample, the landslide group can be considered representative from the geomorphological point of view, and can be used for prediction purposes. The landslide areas (mean size, 6,544 m2; total, 137,415 m2) and, particularly, the landslide volume (mean, 14,650 m3; total, 307,653 m3) show the considerable potential economic significance of rotational slides in the test site. In fact, rotational movements have been responsible for damage to property and built structures (mainly roads) in recent years.

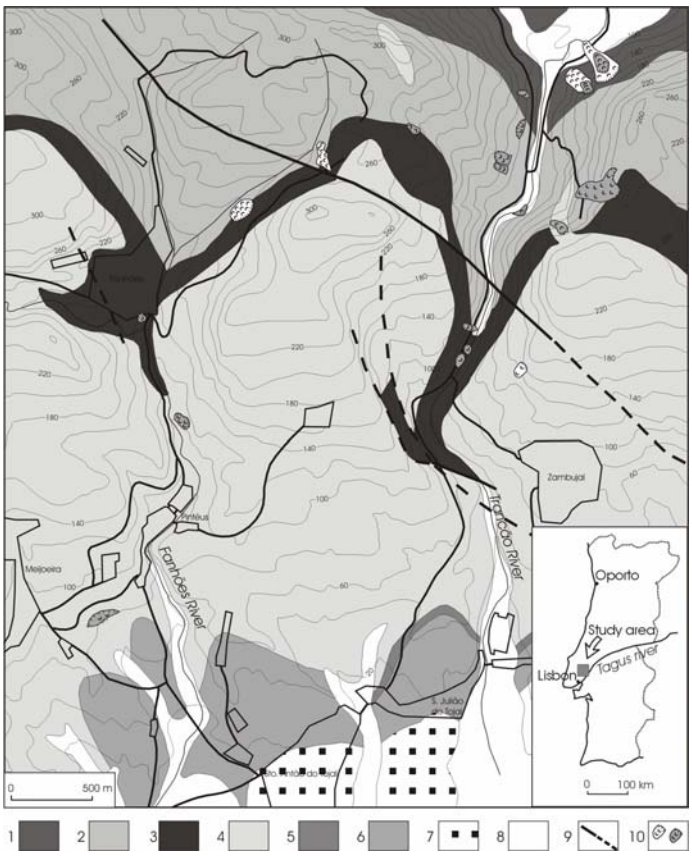

Figure 1. Geological map of the Fanhões-Trancão test site and spatial distribution of rotational slides.
1. Upper Barremian – Aptian sandstones; 2. Albian – Middle Cenomanian marls and marly limestones; 3. Upper Cenomanian limestones; 4. Upper Cretaceous Volcanic Complex of Lisbon; 5. Paleogene lacustrine limestones; 6. Paleogene conglomerates and sandstones; 7. Quaternary terraces; 8. Alluvial plain; 9. Fault (uncertain - dashed); 10. Rotational slides (white, age ≤ 1967; grey, age > 1967).

3 METHODOLOGY

3.1 Susceptibility assessment

Landslide susceptibility assessment is based on the assumption that the likelihood of landslide occurrence can be measured by statistical relationships between past landslides of a given type and spatial data sets of given variables. Therefore, it is assumed that all landslides occurred under particular conditions that can be characterized by these spatial data sets, which are considered as predisposing or conditioning factors. Table 1 summarizes the number of classes in each of the seven landslide conditioning factors, as well as the data capture procedures. The thematic layers were imported to ILWIS 3.1 and rasterized for analytical purposes. A pixel size of 5 m (25 m^2) was used, and therefore, the test site corresponds to 949 x 841 pixels (total area = 798,109 pixels).

Table 1. Thematic layers used for landslide susceptibility assessment.

Variable	Number of classes	Data capture
Slope angle	8	Derived from DEM (pixel 5 m).
Slope aspect	9	Derived from DEM (pixel 5 m).
Transversal slope profile	5	Directly drawn on a 1:2000 scale topographic map (5 m contour).
Lithology	6	Geological map (1:50,000); validation with aerial photo interpretation and field work.
Superficial deposits	7	Field work; detailed geomorphological mapping (1:2000).
Geomorphological units	11	Directly drawn on a 1:2000 scale topographic map (5 m contour).
Land use	6	Interpretation of a digital orthophoto map at a scale 1:10,000; field work verification.
Landslide distribution		Field work; detailed geomorphological mapping (1:2000).
Nr. of classes	52	

Data integration of all variables was made using the Joint Conditional Probability Function (Chung et al., 1995; Zêzere et al., 2004), applied over 15,636 unique condition sub-areas obtained by the overlay of all thematic layers. The data integration was applied to the total set of rotational slides, and a favourability value (susceptibility indicator) ranging from 0 to 1 was computed for each pixel of the area.

3.2 Validation and classification of susceptibility

To validate the prediction results, the landslide data set was partitioned using different criteria: temporal, spatial and random. Table 2 summarizes the seven selected validation strategies. The first sub-set (estimation group) was used to obtain a prediction map. The second sub-set (validation group) was compared with the prediction results for validation, after sorting in descending order the 798,109 susceptibility values, one per each pixel (Fig. 2). The computed prediction-rate curves can be used to interpret and classify the susceptibility map obtained taking in account the complete landslide data set of rotational slides, as proposed by Chung & Fabbri (in press).

3.3 Landslide triggering and frequency analysis

Transformation of susceptibility in hazard implies the availability of information about expected num-

ber and expected size of future landslides that are to occur within a specified time period (Chung & Fabbri, in press). Such extrapolation was obtained for the study area through landslide frequency analysis.

Table 2. Strategies developed for validation of landslide susceptibility assessment.

Partition criteria	Estimation group	Validation group	Format of results
No data partition	Total landslide data set	Total landslide data set	Success-rate
Temporal [1]	Landslide age ≤ 1967	Landslide age > 1967	Prediction-rate
Temporal [2]	Landslide age ≤ 1979	Landslide age > 1979	Prediction-rate
Temporal [3]	Landslide age ≤ 1983	Landslide age > 1983	Prediction-rate
Spatial [1]	Fanhões sub-set	Trancão sub-set	Prediction-rate
Spatial [2]	Trancão sub-set	Fanhões sub-set	Prediction-rate
Random	Random [1] sub-set	Random [2] sub-set	Prediction-rate

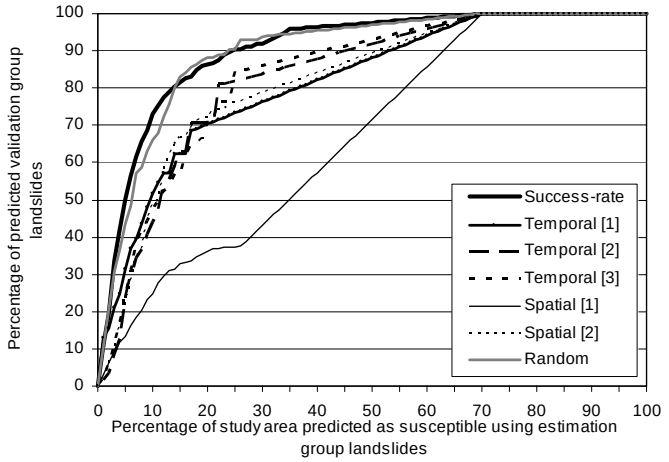

Figure 2. Success-rate and prediction-rate curves of the susceptibility assessment of rotational slides.

Slope movements in the test site have a clear climatic signal, as confirmed by the large number of landslides triggered during the wettest years, and by the general stability of slopes during most of the remaining years (Zêzere et al., 1999; Zêzere, 2000; Zêzere & Rodrigues, 2002). Table 3 summarizes the recognized dates of past rotational slides within the test site, and the total unstable area calculated for each of the rainfall triggered landslide events.

Rainfall was related with the historic occurrence of landslides through the reconstruction of cumulative rains from 1 to 90 days for the periods of major slope instability observed during the last four decades in the study area. The return periods of obtained intensity-duration combinations were calculated applying the Gumbel law. Critical pairs of rainfall amount-duration were defined assuming as critical values the extreme combinations from the statistical point of view. The obtained results are summarized in Table 4, where the critical rainfall amount-durations are highlighted in bold.

Table 3. Age of rotational slides and total affected areas in the Fanhões-Trancão test site.

Age	N	(%)	Total affected area (m^2)	(%)
1967 or prior	5	23.8	60,348	43.9
1979, February	3	14.3	15,923	11.6
1983, November	3	14.3	11,236	8.2
1989, November	1	4.8	1,781	1.3
1996, January	9	42.9	48,127	35.0
Total	21	100.0	137,415	100.0

Table 4. Cumulative rainfall from 1 to 90 days and return periods for the rotational slide events recognized in the Fanhões-Trancão test site (rainfall data from S. Julião do Tojal, period: 1956-2001; R – rainfall (mm); R.P. – return period (years).

Days		1967 Nov.25	1979 Feb.10	1983 Nov.18	1989 Nov.25	1996 Jan.28
1	R (mm)	**137.0**	26.0	**163.7**	38.0	25.5
	R.P. (y)	**60**	1.1	**200**	1.4	1.1
5	R (mm)	141.5	137.9	230.3	91.3	47.9
	R.P. (y)	5.5	4.5	65	1.7	1
10	R (mm)	155.7	160.5	265.2	164.7	119.8
	R.P. (y)	3	3	25	3.5	1.7
15	R (mm)	176.9	203.5	349.9	**216.5**	153.2
	R.P. (y)	2.5	3.5	38	**4.5**	1.8
30	R (mm)	248.5	335.2	403.7	217.6	361.3
	R.P. (y)	2.5	5.5	13	1.8	7.5
40	R (mm)	307.4	351.1	407.3	277.7	**495.2**
	R.P. (y)	3	4	7	2.2	**20**
60	R (mm)	307.4	532.8	407.3	340.0	596.1
	R.P. (y)	1.8	9.5	3.5	2.2	15
75	R (mm)	309.9	**693.7**	407.3	350.8	684.7
	R.P. (y)	1.7	**20**	2.7	2	18
90	R (mm)	309.9	694.2	407.3	351.5	758.7
	R.P. (y)	1.4	13	2	1.6	19

The temporal dimension of landslide hazard is achieved through the assumption that the rainfall combination (amount-duration) that produced slope instability in the past will produce the same effects every time they occur in the future (i.e. same type of landslides and similar total affected area). As the return periods of such triggering events are known, different scenarios can be modelled, each one corresponding to a specific return period.

4 RESULTS AND DISCUSSION

Results from the success-rate curve presented in Figure 2 are very promising, since the 10% area predicted as more susceptible (*x axis*) includes 73% of the total area affected by landslides (*y axis*), and this value grows to 90%, when the 25% area of highest susceptibility is considered. The prediction-rate curve obtained with the random partition of the landslide data set, also shows very good results, quite similar to the previous one. Nevertheless, these two curves are not the best ones to validate the susceptibility assessment. In the first case, the success-rate curve has limitations, since it arises from the comparison between the prediction map and the same landslide data set that was used to generate it. In the second case, although different landslide sub-

sets were used to construct the susceptibility model and to validate it, no temporal or spatial criteria were considered in the partition procedure. Empirical experience has shown that in such cases the validation results tend to be overestimated (Chung & Fabbri, in press).

The prediction-rate curves computed with the landslide data set partitioned with spatial criteria show interesting results (Fig. 2). The susceptibility model constructed with the landslides of the Trancão sub-basin is able to predict well the rotational slides that occurred in the Fanhões sub-basin (72% of the landslide validation group is included within the 20% most susceptible area, as shown by spatial [2] curve). However, the landslides from Fanhões, show poor results in the prediction of the susceptibility in the Trancão sub-basin (the 20% area with highest susceptibility includes only 36% of the landslide validation set, as shown by spatial [1] curve). The latter seems to be justified by: (i) the strong spatial correlation between rotational slides and sandstones of Upper-Barremian age, which outcrop within the Trancão sub-basin, but not in the Fanhões sub-basin (Fig. 1); and (ii) the importance of steep slopes as a landslide predisposing factor in the Trancão sub-basin.

Finally, three different temporal partitions were tested (Table 2), and the computed prediction-rate curves are very similar (Fig. 2). The curve corresponding to the temporal partitioning in 1967 (temporal [1]) was selected for the landslide susceptibility validation, because it presents the best results for the highest susceptibility areas. This prediction-curve is then used to interpret and classify the first susceptibility map produced with the total set of rotational slides of the test site, as proposed by Chung & Fabbri (in press).

Table 5 presents the prediction results of susceptibility modelling corresponding to the temporal [1] prediction-curve. The interpretation of such data allows the identification of the following landslide susceptibility classes:

(I) The 1st and highest susceptibility class, covers only 1% of the study area (8,122 pixels) and includes 13% of the area of the landslide validation group;

(II) The 2nd susceptibility class covers 11% of the study area (88,934 pixels) and includes 45% of the area of the landslide validation group;

(III) The 3rd susceptibility class covers 5% of the study area (40,334 pixels) and includes 11% of the area of the landslide validation group;

(IV) The 4th susceptibility class is the largest in area (423,765 pixels corresponding to 53% of the total area) and includes 31% of the area of the landslide validation group;

(V) The less susceptible class includes 30% of the study area (236,954 pixels) and has no relationship with the landslide validation group.

The highest susceptibility class doesn't contain the highest percentage of the landslide validation group, but it really defines the most susceptible area, considering the existing differences among absolute areas covered by the five susceptibility classes.

Table 5. Prediction results of susceptibility assessment based on a temporal partition (Temporal [1]) of the rotational slides data set.

Area classified as susceptible (%)	Absolute frequency of landslide validation group	Cumulative frequency of landslide validation group	Landslide susceptibility classes
Top 1%	12.75	12.75	I
1-2	2.91	15.66	
2-3	5.47	21.13	
3-4	3.75	24.88	
4-5	6.47	31.35	
5-6	5.69	37.04	
6-7	2.49	39.53	II
7-8	4.02	43.55	
8-9	4.36	47.91	
9-10	3.82	51.73	
10-11	3.04	54.77	
11-12	2.46	57.23	
12-13	0.00	57.23	
13-14	4.95	62.18	
14-15	0.00	62.18	III
15-16	0.00	62.18	
16-17	6.34	68.52	
17-18	0.59	69.11	
18-19	0.59	69.71	IV
……	……	……	
69-70	0.59	100	
70-100	0.00	100	V

The previously defined limits of 1%, 12%, 17% and 70% of the study area, identified according to the prediction results obtained with the temporal[1] partition of the landslide database, were used to classify and interpret the susceptibility map computed with the total rotational slide data set and the result is presented in Figure 3.

Assuming that relationships between future slope movements and landslide predisposing factors will be similar to those verified in the past, we are able to predict that future rotational slides occurring in a non-specified time span, will be distributed through the susceptibility classes according to the values obtained from the prediction-rate curve temporal [1] (Fig. 2; Table 5). Therefore, 13%, 45%, 11% and 31% of the future rotational movements will be located in the susceptibility classes I, II, III and IV, respectively, while the susceptibility class V will not be affected by rotational movements.

If we assume now that critical pairs of rainfall amount-duration that produced rotational slides within the test site in the past, will originate similar total affected areas every time they occur in the future (Table 3), different hazard scenarios can be assessed. As the return period of the triggering events is known (Table 4), each hazard scenario will correspond to a specific return period.

Figure 3. Rotational slide susceptibility map of the Fanhões–Trancão test site, classified according to the prediction-rate curve obtained with the temporal partition of the landslide data set *temporal [1]*. I, II, III, IV, V – landslide susceptibility classes; RS – Rotational slides.

The conditional probability of a pixel to become affected by a rotational slide in the future is computed for each particular scenario, taking in account the information of the relevant prediction-rate curve, as well as the classes of the susceptibility map (Zêzere et al., 2004):

$$P = 1 - \left(1 - \frac{Taffected}{Ty} . pred\ y\right) \quad (1)$$

where *Taffected* = total area to be affected by rotational slides in a scenario (*x*); *Ty* = total area of susceptibility class *y; pred y* = prediction value of susceptibility class *y*.

Table 6 shows the results obtained for three specific rainfall triggering scenarios: (1) 694 mm in 75 days (20-year return period - February 1979); (2) 217 mm in 15 days (4.5–year return period – No-

vember 1989); and (3) 495 mm in 40 days (20–year return period - January 1996).

Table 6. Calculation of probabilities for the hazard assessment of rotational slides on a scenario basis.

Landslide susceptibility class	Area (number of pixels) (pixel= 5m)	Predictive value of susceptibility class	Probability to each pixel to be affected by a landslide — Scenarios (1) Feb. 1979	(2) Nov. 1989	(3) Jan. 1996
I - Top 1%	8122	0.1275	0.0100	0.0011	0.0302
II – 1-12%	88934	0.4448	0.0032	0.0004	0.0096
III - 12-17%	40334	0.1129	0.0018	0.0002	0.0054
IV - 17-70%	423765	0.3148	0.0005	0.0001	0.0014
V – 70-100%	236954	0.0000	0.0000	0.0000	0.0000

The mapping of the probabilities summarized in Table 6 enables the production of three different hazard scenarios, each one related to a particular rainfall combination with a defined return period. While the spatial distribution of susceptibility classes remains unchanged in all hazard scenarios, significant differences are to be found on the probability for each pixel to be affected by a rotational slide, and on the related return period. It is significant to note that quite different landslide hazard scenarios can be produced using different rainfall amount-duration combinations with the same return period, as is confirmed by the differences on probabilities within scenarios (1) and (3), which have the same return period (20 years).

5 CONCLUSION

Evaluation of spatial correlation between landslides of a specific typology and instability predisposing factors is a critical step for landslide susceptibility assessment. Moreover, the evaluation of the predictive power of the susceptibility models, as well as the comprehensive definition of susceptibility classes, can be achieved through a validation procedure based on the partitioning of the original landslide data set. Finally, if slope movements are mostly induced by rainfall, as it is the case discussed in this paper, the landslide frequency analysis can be coupled with the statistical treatment of rainfall data, and results can be incorporated in the modelling procedure towards landslide hazard assessment.

The coupling between the susceptibility map, prediction-rate curve and critical rainfall (amount-duration) triggering events allows the evaluation of landslide hazard as the probability of each pixel to be affected by a rotational slide, on a scenario basis. These probabilistic data can be easily integrated with vulnerability information of the study area, in order to go further on the landslide quantitative risk analysis.

ACKNOWLEDGEMENTS

This paper is part of the European Commission project “Assessment of Landslide Risk and Mitigation in Mountain Areas, ALARM” (contract EVG1-CT-2001-00038), Fifth Framework Programme.

REFERENCES

Aleotti, P. & Chowdhury, R. 1999. Landslide hazard assessment: summary review and new perspectives, *Bull. Eng. Geol. Env.*, 58: 21-44.

Carrara, A.; Guzzetti, F.; Cardinali, M. & Reichenbach, P. 1998. Current limitations in modelling landslide hazard. In Buccianti, A.; Nardi, G. & Potenza, R. (eds.), *Proceedings of IAMG'98*: 195-203.

Chung, C.F. & Fabbri, A. 2003. Validation of Spatial Prediction Models for Landslide Hazard Mapping. *Natural Hazards*, 30 (3): 451-472.

Chung, C.F.& Fabbri, A. in press. Systematic procedures of landslide-hazard mapping for risk assessment using spatial prediction models. In Glade, T.; Anderson, M.G. & Crozier, M.J. (eds.) *Landslide Hazard and Risk*, London: John Wiley & Sons Ltd.

Chung, C.F.; Fabbri, A. & Van Westen, C.J. 1995. Multivariate regression analysis for landslide hazard zonation. In, Carrara, A. & Guzzetti, F. (eds.), *Geographical Information Systems in Assessing Natural Hazards*: 107-133. Dordrecht: Kluwer Academic Publishers.

Fabbri, A.; Chung, C.F.; Napolitano, P.; Remondo, J. & Zêzere, J.L. 2002. Prediction rate functions of landslide susceptibility applied in the Iberian Peninsula. In Brebbia, C.A. (ed.), *Risk Analysis III*, Series: Management Information Systems vol. 5: 703-718. Southampton: WIT Press.

Hansen, A. 1984. Landslide hazard analysis. In Brunsden, D. & Prior, D.B. (eds.), *Slope Instability*: 523-602. Chichester: John Wiley & Sons.

Hutchinson, J.N. 1995. Landslide hazard assessment, keynote paper. In Bell (ed.), *Landslides, Proceedings of the 6th International Symposium on Landslides*: 1805-1841. Rotterdam: Balkema.

Soeters; R. & Van Westen, C.J. 1996. Slope Instability Recognition, Analysis and Zonation. In Turner, A.K. & Schuster, R.L. (eds.), *Landslides. Investigation and Mitigation*. Transportation Research Board, Special Report 247: 129-177. Washington D.C.: National Academy Press.

Varnes, D.J. & International Association of Engineering Geology Commission on Landslides and Other Mass Movements on Slopes. 1984. *Landslide hazard zonation: a review of principles and practice*. Paris: UNESCO.

Zêzere, J.L. 2000. Rainfall triggering of landslides in the Area North of Lisbon. In Bromhead, E.; Dixon, N. & Ibsen, M.-L. (eds.), *Landslides in Research, Theory and Practice*, vol. 3: 1629-1634. London: Thomas Telford.

Zêzere, J.L.; Ferreira, A.B. & Rodrigues, M.L. 1999. Landslides in the North of Lisbon Region (Portugal): Conditioning and Triggering Factors. *Physics and Chemistry of the Earth (Part A)*, 24 (10): 925-934.

Zêzere, J.L. & Rodrigues, M.L. 2002. Rainfall Thresholds for Landsliding in Lisbon Area (Portugal). In Rybar, Stemberk & Wagner (eds.), *Landslides*: 333-338. Lisse: Balkema.

Zêzere, J.L.; Reis, E.; Garcia, R.; Oliveira, S.; Rodrigues, M.L.; Vieira, G. & Ferreira, A.B. 2004. Integration of spatial and temporal data for the definition of different landslide hazard scenarios in the Area North of Lisbon (Portugal). *Natural Hazards and Earth System Sciences*, European Geosciences Union, 4: 133-146.